Enhanced fault tolerance in biomimetic hierarchical materials: A simulation study

Seyyed Ahmad Hosseini, * Paolo Moretti, and Michael Zaiser
Institute of Materials Simulation (WW8), Friedrich-Alexander-Universität Erlangen-Nürnberg, Dr.-Mack-Strasse 77, 90762 Fürth, Germany

(Received 19 November 2022; revised 3 May 2023; accepted 9 May 2023; published 26 May 2023)

Hierarchical microstructures are often invoked to explain the high resilience and fracture toughness of biological materials such as bone and nacre. Biomimetic material models inspired by such hierarchical biomaterials face the obvious challenge of capturing their inherent multiscale complexity, both in experiments and in simulations. To study the influence of hierarchical microstructure on fracture properties, we propose a large-scale three-dimensional hierarchical beam-element simulation framework, in which we generalize the constitutive framework of Timoshenko beam elasticity and maximum distortion energy theory failure criteria to the complex case of hierarchical networks of up to six self-similar hierarchical levels, consisting of approximately 5 million elements. We perform a statistical study of stress-strain relationships and fracture surface morphologies and conclude that hierarchical systems are capable of arresting crack propagation, an ability that reduces their sensitivity to preexisting damage and enhances their fault tolerance compared to reference fibrous materials without microstructural hierarchy.

DOI: 10.1103/PhysRevMaterials.7.053612

I. INTRODUCTION

Hierarchically structured materials display self-similar morphology in which comparable microstructural features are reproduced on multiple scales. A global tendency of biological systems to be organized in a hierarchical modular fashion is evident, for instance, in the case of collagen, which contains hierarchically structured patterns, from the molecular scale of amino acid chains, through microfibrils and fibers, up to hierarchical fiber bundles. This arrangement ensures enhanced fracture toughness over assemblies of isolated collagen molecules [1] and is believed to play a major role, for instance, in bone fractures [2,3]. Similar considerations have been proposed to explain and characterize the cellular structure of wood [4] and hierarchical lamellar microstructures of mollusk shells (nacre) [5]. In this broad context, hierarchical structures are believed to control internal load redistribution in a manner that contains local damage, thus enhancing resilience even in materials with brittle constituents [6,7].

The possibility of engineering hierarchical biomimetic structures, which are fault tolerant regardless of the inherent unreliability of their constituents, or the fluctuations in their constitutive behavior is, of course, very appealing from the point of view of (bio)material synthesis and design. While the preponderant role of the hierarchical structure is a gross simplification when addressing real biological materials like bone, it could prove useful in the context of biomimetic materials, in which one wants to control fracture behavior, rather than model a complex biological system. The mechanisms of synthesis and growth of materials which are known to exhibit hierarchical microstructures, such as nacre, can sometimes be observed in controlled laboratory environments [8]. However, experimental growth via nanoassembly processes leads to structures that rarely exhibit hierarchical features beyond the microscale. In the context of biomimetics, hierarchical morphology may be obtained via other routes such as additive manufacturing, which allow one to access much larger scales for the structural features. In this case, even without a detailed understanding of the biomechanochemistry of self-assembly processes in biological systems, the geometrical freedom inherent in additive manufacturing processes allows one to construct complex microstructures. Moreover, simulation methods can be used to model and tune such structures in order to enhance their performance in view of specific load-carrying applications, possibly even beyond the possibilities attainable via self-assembly routes.

Here, we propose a large-scale numerical study of bulk fracture in three-dimensional (3D) fibrous hierarchical structures and show that, even under minimal assumptions, systems of this type exhibit a unique fracture behavior in which the nucleation of microcracks is not followed by their expansion or propagation. While previous studies have highlighted this behavior in simplified two-dimensional (2D) models [9] and experiments on sheet materials [10] and/or by resorting to simplified constitutive laws [11–13], our work here is the first study in which a realistic, large-scale, beam-element simulation framework is implemented to provide exhaustive evidence of the enhanced fault tolerance of 3D hierarchical structures.

Regarding numerical models of failure in hierarchical systems, fiber bundle models are among the simplest tools to examine collective phenomena in deformation and fracture [14] and have been widely used to study disordered fibrous materials. The material is modeled as a collection of load-bearing fibers that, in the simplest example of a brittle fiber bundle, elastically deform until they fail at a critical load. The local constitutive behavior can be modified, beyond the ideal brittleness of individual fibers, to incorporate gradual damage accumulation [15], creep [16], and plasticity [17].

*ahmad.hosseini@fau.de

Importantly, hierarchical generalizations of such models have also been proposed [18,19]. However, fiber bundle models are not intended to investigate how stress is spatially (re)distributed across a material, nor can they clearly tell if failure is caused by the growth of a local nucleus triggered by stress concentrations, damage percolation across the entire system, or some intermediate mechanism. As a consequence, studies of fiber bundle models have devoted comparatively little attention to the fundamental topic of the nature of the failure process [14].

On the lowest structural level, fracture of hierarchical materials can be modeled using atomistic methods. These simulations may subsequently be used to parametrize mesoscale models that describe behavior at higher hierarchical levels [20]. Alternatively, they may be taken to include several hierarchical levels in extremely large-scale simulations [1], where computational cost can limit access to larger sizes.

Lattice/network models represent a viable alternative to efficiently capture multiple hierarchical levels and length scales. Discrete lattice models for materials fracture were introduced to study the statistical effects of microstructural disorder (more precisely, fluctuating local strength) [21]. In models like the random-fuse model (RFM), the random-spring model, and the random-beam model, materials are represented as networks of discrete elements that transmit scalar, vector, or tensor loads. Such models serve as paradigms for fracture as a multiscale process, capturing its key features such as the interplay between local failure, microstructural heterogeneity (represented, e.g., in terms of locally random network architecture or statistically distributed failure thresholds of individual elements), and system-spanning interactions as the load redistributes across the network. Such models attain a level of simplicity that allows for large-scale simulations and statistically meaningful predictions [22]. Original lattice models of biomimetic structures, inspired, for instance, by nacre, resorted to RFM simulations and their simplifying assumptions of scalar loads and scalar constitutive laws [23], although without considering the material's hierarchical structure [24]. These models were later generalized to account for tensorial loads, in which both elastic equilibrium equations and constitutive laws take into account the local balance of linear and angular momenta [25]. More recently, similar beam lattice models have been used to explore optimal network arrangements in view of fracture behavior [26] and, in particular, to investigate biomimetic 2D hierarchical structures.

In this study, we introduce a 3D hierarchical beam lattice model to explore how the hierarchical organization affects the fracture properties of biomimetic fibrous materials. We compare the crack sensitivity of hierarchical structures to that of reference, nonhierarchical systems. Finally, we compare the characteristics of failure and morphology of fracture surfaces to understand how the microstructure contributes to the enhanced mechanical performance of hierarchical systems.

II. METHODS

Our lattice model is based on a cubic lattice of interconnected beams clamped together at their intersections. The points where beams are mutually connected are called nodes, and we assume L^3 nodes are arranged in a simple cubic lattice structure forming a cube whose edge length L is referred to as the lattice size. The simulations in this study are performed on lattices of size $L = 128$, which are subject to tensile loads directed parallel to one of the cube edges which we identify with the z axis of a Cartesian coordinate system (see Fig. 1). Beams with the same orientation as the load axis are called load-carrying (LC) beams, their number is denoted as N_{LC}, and a set of l connected LC beams is referred to as a LC *fiber* of length l. In contrast, beams oriented perpendicular to the load axis are called cross-link (CL) beams, their number is denoted as N_{CL}, and a set of l connected CL beams is referred to as a CL *connector* of length l. Finally, a connected area with the normal vector perpendicular to the z axis across which all CL beams are missing is denoted as a *gap*. According to our nomenclature, CL connectors are extended chains that may contribute to load redistribution among LC fibers, while gaps are extended surfaces that interrupt it.

A. Construction of 3D hierarchical and nonhierarchical beam lattices

In order to visualize the structure of a deterministic hierarchical beam lattice (DHBL) we devise an iterative "bottom-up" method, as shown in Fig. 1. [Note that, in the global coordinate system defined in Fig. 1, the position vector coordinates $(\bar{x}, \bar{y}, \bar{z})$ carry overbars in order to distinguish them from local coordinates in a beam coordinate system used, e.g., in Fig. 3 below. The same notation convention is used for other quantities such as displacement and force vector or stiffness matrices.]

A level-1 module, or generator, is the basic building block of the hierarchical structure, constituted by a CL plane and eight LC beams. At every iterative step n, this structural pattern is replicated in the form of a (periodically continued) CL plane of linear size 2^n and eight LC superbeams, each corresponding to a level-$(n-1)$ system.

This construction results in a hierarchical arrangement of modules separated by gaps and connected by CL connectors. In the DHBL pattern, as well as in analogous 2D structures [11], the linear sizes of gaps are power law distributed. The structure of the model is deterministic in the sense that its connectivity features at every location can be deduced from the location itself, with no random deviations. Stochastically shuffled versions of these structures have been proposed in the literature in the context of 2D models [9,11]. While shuffled hierarchical structures lend themselves better to statistical studies that require averaging across thousands of network realizations, their behavior is, for 2D structures, essentially identical to those of their deterministic counterparts [9]. For this reason, here, we focus on deterministic hierarchical beam lattices while also simulating a stochastically shuffled 3D hierarchical beam lattice (SHBL) to demonstrate that the conclusions regarding analogous behavior of SHBL and DHBL obtained from 2D systems carry over to three dimensions (see the video in the Supplemental Material [27]).

For comparison with these hierarchical structures, we introduce randomized nonhierarchical reference patterns as follows. A random beam lattice (RBL) of size $L = 2^n$ is constructed from the same number of N_{LC} beams and N_{CL}

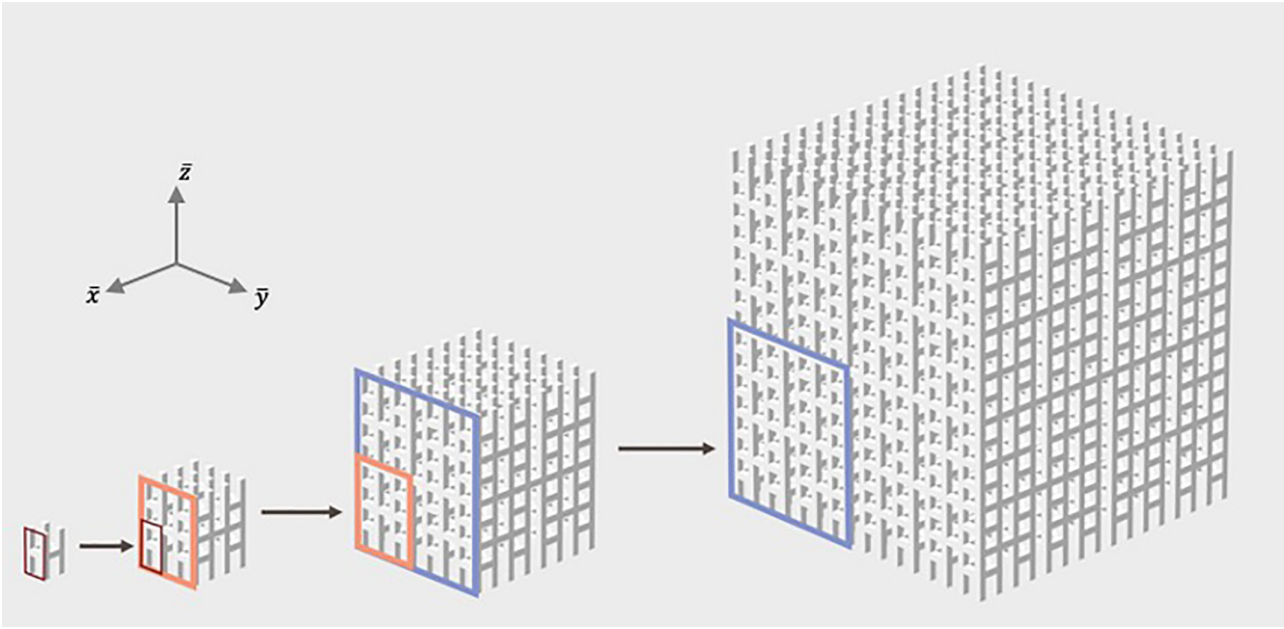

FIG. 1. Iterative "bottom-up" construction of a hierarchical lattice. A module of level 1 ("generator") consists of eight LC beams, plus a CL pane of four load-perpendicular (here, horizontal) beams. Level-n systems are constructed by increasing the system size by powers of 2 and replicating the same $8 + 4$ pattern, where the eight new LC superbeams are now modules which mimic level-$(n - 1)$ systems. Here, we show all the cases up to $n = 4$.

cross-links as the corresponding DHBL, but the CL beams are distributed randomly over the possible CL sites, leading to an exponential distribution of the gap linear sizes. Every realization of our RBL consists of a different random rearrangement of cross-links.

In order to compute fracture toughness, we also consider systems with preexisting flaws in the form of planar cracks of length a. As depicted in Fig. 2, lattices with preexisting cracks are modeled through a set of aL missing adjacent LC beams at locations $x_0 \leqslant \bar{x} \leqslant x_0 + a$, $0 \leqslant \bar{y} \leqslant L$, $\bar{z} = z_0$, where $0 \leqslant a < L$ is the crack length and (x_0, z_0) are the coordinates of the left crack end point in the $\bar{x}\bar{z}$ plane.

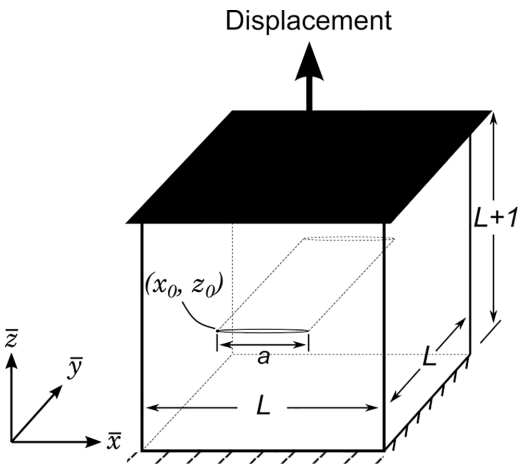

FIG. 2. Schematic of simulations on precracked samples. Periodic boundary conditions are applied on the free sides of the samples.

B. Material model

The constituents of the lattice model are assumed to be straight, identical beams of unit modulus of elasticity, unit length, and square cross section, which are capable of resisting axial and shear forces and bending moments. There are six degrees of freedom (DOFs) at each node, including three translational DOFs (node displacements u, v, and w along the x, y, and z axes, respectively) and three rotational DOFs (rotation angles θ_x, θ_y, and θ_z about the x, y, and z axes, respectively), as illustrated in Fig. 3.

The beams are assumed to show linear elastic mechanical behavior, and Timoshenko beam theory describes their deformation by relating the forces and moments to the associated displacements (see [28] for a more detailed review of the beam theory and the governing equations). Considering a local coordinate system aligned with each beam's axis (see Fig. 3), the displacements and rotations of the beam end nodes are assembled into a local displacement vector $\boldsymbol{u}$, and the forces and moments acting on the end nodes are assembled into a local force vector $\boldsymbol{F}$, resulting in $\boldsymbol{Ku} = \boldsymbol{F}$ for all beams. An

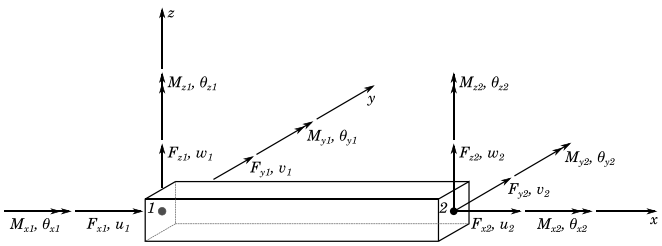

FIG. 3. Beam element with generalized displacements and forces.

explicit expression for a Timoshenko beam's local stiffness matrix $\boldsymbol{K}$ is available in the literature [29].

Assuming quasistatic deformation, we neglect inertial forces. Thus, the global force balance equation of the entire lattice takes the form $\bar{\boldsymbol{K}} \cdot \bar{\boldsymbol{u}} = \bar{\boldsymbol{F}}$, where $\bar{\boldsymbol{u}}$ (the global displacement vector) includes all nodal displacements and rotation angles and $\bar{\boldsymbol{F}}$ includes the external forces in the global coordinate system. The global stiffness matrix $\bar{\boldsymbol{K}}$ is formed by first transforming the local stiffness matrices of all lattice beams into the global coordinate system and then assembling them into $\bar{\boldsymbol{K}}$.

C. Failure criterion

We assume that beams fail irreversibly once a stress-based failure criterion is met. Since the loads on each beam are applied through the end nodes and the beam is in quasistatic equilibrium with small deformations, the magnitudes of forces at the beam ends are equal with opposite directions, and the bending moments vary linearly along the beam. Therefore, the beam's stress is maximum at one end, allowing us to check the failure criterion only at the beam end surfaces. We choose a beamwise failure criterion based on maximum distortion energy theory (von Mises) as follows:

$$\sigma = \sqrt{\sigma_{xx}^2 + 3\left(\sigma_{xy}^2 + \sigma_{xz}^2\right)} = t, \tag{1}$$

where t is the equivalent stress at failure (beam failure threshold). The axial stress σ_{xx} in Eq. (1) consists of tensile/compressive and bending components, which at the beam end surface with outward normal $\boldsymbol{n}$ are given by

$$\sigma_{xx} = \frac{\boldsymbol{F} \cdot \boldsymbol{n}}{A} + \frac{M_z y}{I_z} + \frac{M_y z}{I_y}, \tag{2}$$

where I_y and I_z are the moments of inertia about the (local) y and z axes, respectively (see Fig. 3). A force $\boldsymbol{F}$ in the direction of the outward normal of the beam end surface ($\boldsymbol{F} \cdot \boldsymbol{n}{=}F_x{>}0$) yields a positive (tensile) stress contribution, and a force in the opposite direction yields a negative (compressive) stress contribution. The shear stresses in Eq. (1), on the other hand, are caused by shear (being maximum at the beam's central axis) and torsional loads (being maximum along the centerline of the beam's outer face) [30,31]:

$$\tau_{\max}(\text{shear}) = \frac{3V}{2A}, \quad \tau_{\max}(\text{torsion}) = \frac{M_x}{cb^3}, \tag{3}$$

where V is the shear force, $A = b^2$ is the cross-sectional area of the beams with sides $b = 1$, and $c = 0.208$ is the maximum shearing stress coefficient for square bars in torsion [31]. We choose the bigger absolute τ value in each transverse direction to be the effective shear component:

$$|\sigma_{xy}| = \max\left(\left|\frac{3F_y}{2A}\right|, \left|\frac{M_x}{cb^3}\right|\right),$$
$$|\sigma_{xz}| = \max\left(\left|\frac{3F_z}{2A}\right|, \left|\frac{M_x}{cb^3}\right|\right). \tag{4}$$

Combining Eqs. (1), (2), and (4), we have the failure criterion

$$\frac{\sigma^2}{t^2} = 1,$$
$$\sigma^2 = \left(\frac{F_x}{A} + \frac{M_z y_{\max}}{I_z} + \frac{M_y z_{\max}}{I_y}\right)^2 + 3\left[\max\left(\left|\frac{3F_y}{2A}\right|, \left|\frac{M_x}{cb^3}\right|\right)^2 + \max\left(\left|\frac{3F_z}{2A}\right|, \left|\frac{M_x}{cb^3}\right|\right)^2\right], \tag{5}$$

which is evaluated at both ends of each beam. If the failure criterion is satisfied, the beam is removed irreversibly. A simplified criterion is obtained by excluding the shear force's contribution to failure, which is commonly employed in the literature (see, e.g., [32]). This simplification, however, contradicts the Timoshenko model for beam deformation and may seriously underestimate the failure likelihood of lateral connector beams, which mainly transmit shear forces.

Beam failure thresholds. To mimic material heterogeneity, the failure thresholds t of beams are randomly assigned using a Weibull probability distribution function with probability density,

$$p(t) = \frac{\beta}{\eta}\left(\frac{t}{\eta}\right)^{\beta-1} \exp\left[-\left(\frac{t}{\eta}\right)^{\beta}\right], \tag{6}$$

with $p(t) \geqslant 0$, $t \geqslant 0$, $\beta > 0$, and $\eta > 0$, where β and η are the distribution's shape and scale parameters, respectively. In this study, we choose $\beta = 4$ to represent a moderate degree of disorder and set $\eta = 1/\Gamma(1 + 1/\beta) \approx 1.103263$ so that the failure thresholds t have a mean value of 1. The investigation of the effects of varying β, in analogy with similar studies for 2D systems [9], is beyond the scope of this work and is being considered for a separate study.

D. Boundary conditions

The external load takes the form of a global displacement in the direction of the LC beams ($\bar{z}$ direction in Fig. 2), imposed through two rigid plates on the top and bottom surfaces of the lattice. Thus, at the lattice's bottom and top nodes, the LC beams are clamped to the rigid plates. Periodic boundary conditions are imposed on the remaining sides of the lattice (i.e., in the $\bar{x}$ and $\bar{y}$ directions).

E. Simulation protocol

Using a displacement control loading scheme, the external displacement increases monotonically until the lattice fails completely. To this end, as illustrated in Fig. 4, a unit external displacement is applied to the upper nodes of the lattice while the lower nodes are fixed (see Fig. 2). The global balance equations ($\bar{\boldsymbol{K}} \cdot \bar{\boldsymbol{u}} = \bar{\boldsymbol{F}}$) are solved to obtain the displacements of all nodes. Then, the global displacements are transformed into the local coordinate system of beams (see Fig. 3) to calculate the local loads using $\boldsymbol{Ku} = \boldsymbol{F}$. Afterwards, the weakest beam is identified as the beam with $(\sigma/t_{ij})_{\max}$. Due to the assumption of small deformations, the beam forces and displacements are homogeneous functions of the first degree of the applied boundary displacement. Thus, scaling the

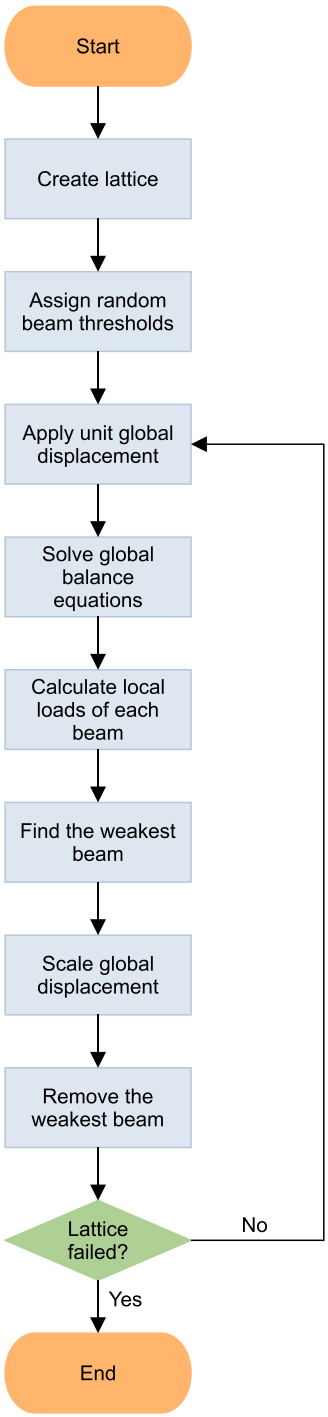

FIG. 4. Simulation protocol.

boundary displacement to $(\sigma/t_{ij})^{-1}_{\max}$ satisfies the failure condition [Eq. (5)] for the weakest beam. However, if this calculated global displacement is less than the displacement d of the previous iteration, d is considered to be the actual global displacement of this iteration. This physically means that the failure at this iteration is triggered by load redistribution after a beam failed in the previous iteration. The weakest beam is then removed, and the loop is repeated if the global failure has not happened. Otherwise, the simulation ends.

We note that the pristine/undamaged systems (both DHBL and RBL) consist, for $n = 6$ hierarchy levels, of 4 860 928 beams, and the corresponding balance equations are a sparse algebraic system with $\approx 1.3 \times 10^7$ unknowns. In the ramp-up to failure, the evaluation of the balance equations is repeated every time a beam is removed. Every data point in the following is obtained by averaging over 10 realizations of the beam network. In each realization, we vary the sequence of thresholds extracted from $p(t)$ and (for only RBL) the random positions of CL beams, as well as the crack position for cracked systems.

III. RESULTS

A. Fracture toughness

To study the effect of hierarchical structure on flaw tolerance, we simulated mode-I-crack propagation in hierarchical (DHBL) and nonhierarchical reference structures (RBL) containing preexisting cracks of varying length $0 \leqslant a < L$ (Fig. 2). As depicted in Fig. 5(a), hierarchical samples exhibit a superrough crack surface, which is reminiscent of fracture patterns in bone [3]. The large deflections in crack profiles indicate that the growth of initially present or newly nucleated cracks is arrested and failure then proceeds by nucleation of new microcracks at other locations of the sample. Only a fraction of these disseminated microcracks ultimately coalesce to form the final fracture surface. Figure 5(d) supports this observation by comparing the fractions λ of broken beams that are *not* part of the final crack surface for DHBL and RBL samples (i.e., they are not part of the minimal set of beams that topologically disconnects the sample). After an initial transient, the fraction of "nonessential" damage in DHBL is nearly double that in RBL. As seen from Fig. 5(c), this results in significant toughening, as the work of failure is increased by the nonessential work needed to create microcracks everywhere in the sample until, ultimately, their percolation produces a system-spanning crack.

Because of this ability to arrest crack growth, hierarchical structures significantly outperform nonhierarchical ones in terms of peak stress and postpeak energy absorption in situations where preexisting cracks of length a are considered, as seen in Figs. 5(b) and 5(c). In nonhierarchical structures, crack growth is driven by the stress concentrations in the fracture process zone, and failure occurs immediately after the system reaches the peak load σ_p:

$$\sigma_p = \frac{K_{Ic}}{\sqrt{\pi(a + a_0)}} f\left(\frac{a}{L}\right), \tag{7}$$

where K_{Ic} is the critical stress intensity factor, a_0 is the process zone size [33], and the function $f(a/L)$ accounts for finite-size effects. Figure 5(b) confirms this picture for our RBL (red data points and red lines), with $f(x) = (x/\tan x)^{1/2}$ and $x = \pi a/(2L)$, as appropriate for a periodic array of mode-I cracks [34]. Here, $K_{Ic} \sim \sqrt{G_c E}$ characterizes the material resistance to fracture and depends on the energy release rate G_c (also known as the fracture toughness) and the elastic modulus E.

As anticipated, in DHBL fracture proceeds differently. The structural gaps, which in this case are power law distributed

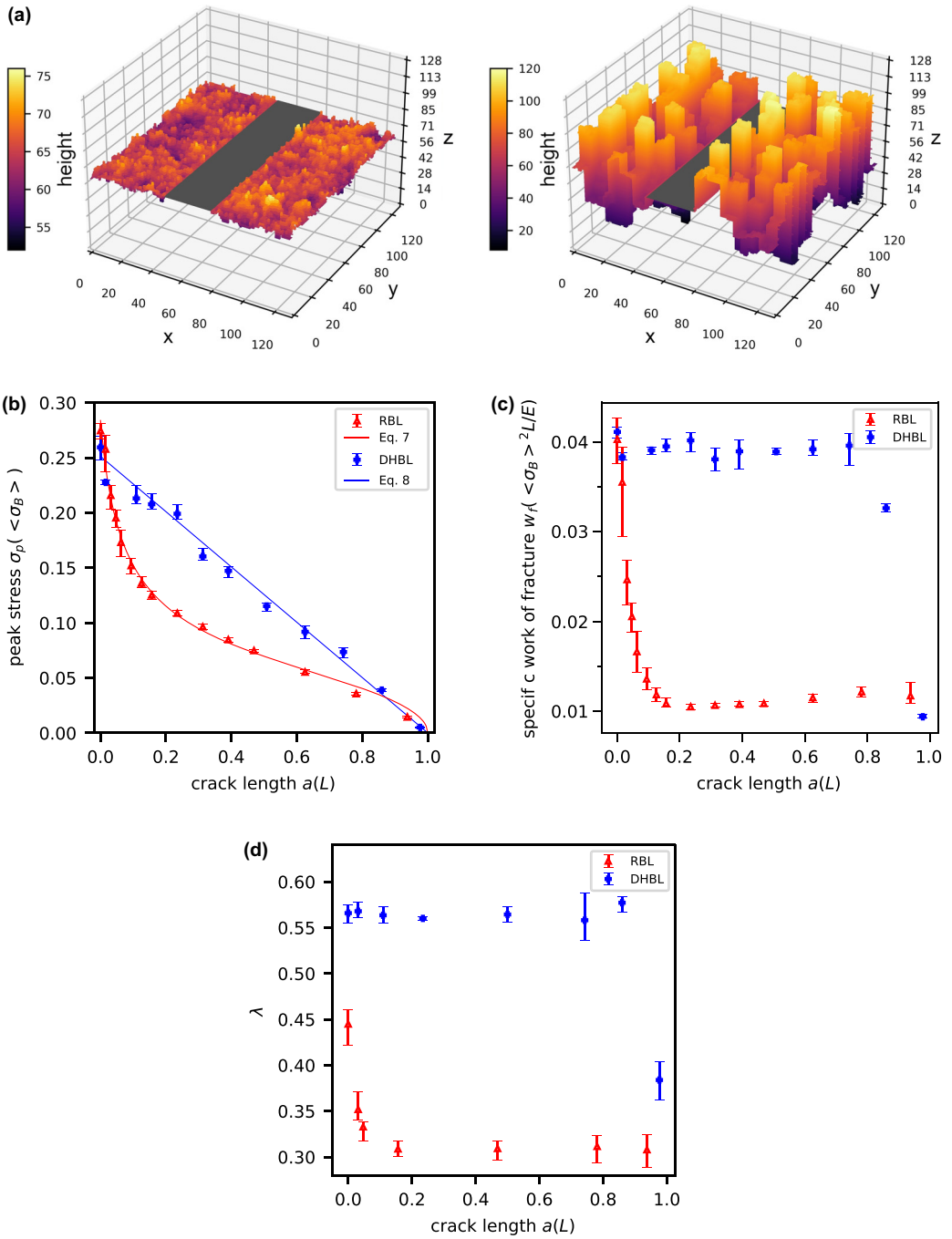

FIG. 5. Simulation results for notched hierarchical (DHBL) and nonhierarchical (RBL) lattice variants of size $L \times L \times L$ with $L = 128$. (a) Typical fracture surface in RBL (left) and DHBL (right); the initial crack of length $a = 30$ is marked in gray, and the color bars indicate height (z coordinate of fracture surface). (b) Peak stress as a function of crack length; all data are averaged over 10 samples, and red and blue lines represent fits according to Eqs. (7) and (8), respectively. (c) Specific work of fracture for the same set of samples. (d) Fraction λ of broken beams that are not on the final crack surface; all data are averaged over 10 samples, and the error bars indicate the corresponding standard deviation.

in size, are responsible for arresting crack propagation and altering long-range stress redistribution. As a consequence, DHBL displays a reduced sensitivity to preexisting cracks, with peak loads that decrease only linearly with the precrack size a as

$$\sigma_p = \sigma_0\left(1 - \frac{a}{L}\right), \tag{8}$$

where σ_0 is the peak stress in the absence of preexisting cracks. In passing, we note that the case of $a \approx 0$ is the only exception, where DHBL falls short of RBL: the relevant aspect of biomimetic hierarchical structures is their ability to cope with preexisting flaws, rather than their peak performance under ideal conditions.

Similar to the maximum load, hierarchical samples may significantly outperform nonhierarchical ones in terms of the

specific work of fracture $w_F = W_F/[L(L-a)]$, defined as the mechanical work W_F needed to fully break the sample from its initial configuration, divided by the initial area $L(L-a)$ of the intact sample cross section. As highlighted in Fig. 5(c), the specific work of fracture of both configurations is independent of crack length after an initial transient, but the saturation level is about a factor of 4 higher for hierarchical samples.

B. Characteristics of fracture surfaces

Absence of crack growth. To confirm our statement that crack growth is arrested in DHBL, we start by looking at damage nucleation and growth patterns of an un-notched sample, as depicted in Fig. 6 for a typical DHBL (left) and RBL (right). Fracture in nonhierarchical materials is caused by the nucleation and propagation of a crack that becomes critical at the system's peak load and spreads throughout the system due to crack-tip stress concentrations, resulting in an abrupt and catastrophic failure. In DHBL, on the other hand, LC modules fail individually, and failure does not propagate to neighboring modules: the vertical deflections indicate that a growing crack has reached a gap and has stopped. The hierarchically distributed gaps inhibit crack propagation at all scales, resulting in widely separated flaws coalescing into a superrough fracture profile in which the crack width in the loading direction is proportional to the system size, resulting in a global roughness exponent of 1.

Crack roughness. The statistical analysis of crack surface patterns allows us to further understand the mechanisms of failure onset and propagation. We consider the fracture surface as the function $\bar{z}(\bar{x},\bar{y})$ in the global coordinate system. We start by computing the crack roughness in terms of the scale-dependent standard deviation,

$$\sigma_r = \left\langle \langle [\bar{z}(\bar{x},\bar{y}) - \langle \bar{z}(\bar{x},\bar{y})\rangle_r]^2\rangle_r^{1/2}\right\rangle_{A,N}, \tag{9}$$

where $\langle\cdots\rangle_r$ denotes the average over a circle of radius r and $\langle\cdots\rangle_{A,N}$ is the average over all circles contained in the sample cross section of area A, as well as over all samples in an ensemble of N simulations with different realizations of a given microstructure.

We investigate the possibility of crack profiles being self-affine. In this context, self-affinity refers to invariance under the scaling transformation $r \to \lambda r, \bar{z} \to \lambda^H \bar{z}$, where H is the Hurst exponent [9]. Self-affinity, in particular via a nontrivial value of H that cannot be inferred from the structure, indicates that the fracture process is affected by emergent features and correlations of the dynamics at hand. Evaluating σ_r allows us to verify whether these scaling relationships hold and to evaluate H when they do.

Figure 7 illustrates the values of σ_r for DHBL and RBL. RBL show a self-affine scaling with a nontrivial Hurst exponent $H = 0.69$, confirming that in heterogeneous nonhierarchical systems growth is controlled by dynamic correlations [21,35]. On the other hand, in DHBL we record an apparent $H = 0.90$. This result can be interpreted as follows: an exponent of 1 derives from the fact that hierarchical lattices with an infinite number of hierarchical levels are invariant under the transformation $\bar{x} \to 2\bar{x}$, $\bar{y} \to 2\bar{y}$, $\bar{z} \to 2\bar{z}$, and the same must be valid for the associated crack profiles. Contrary to the case of RBL, H is compatible with a prediction based

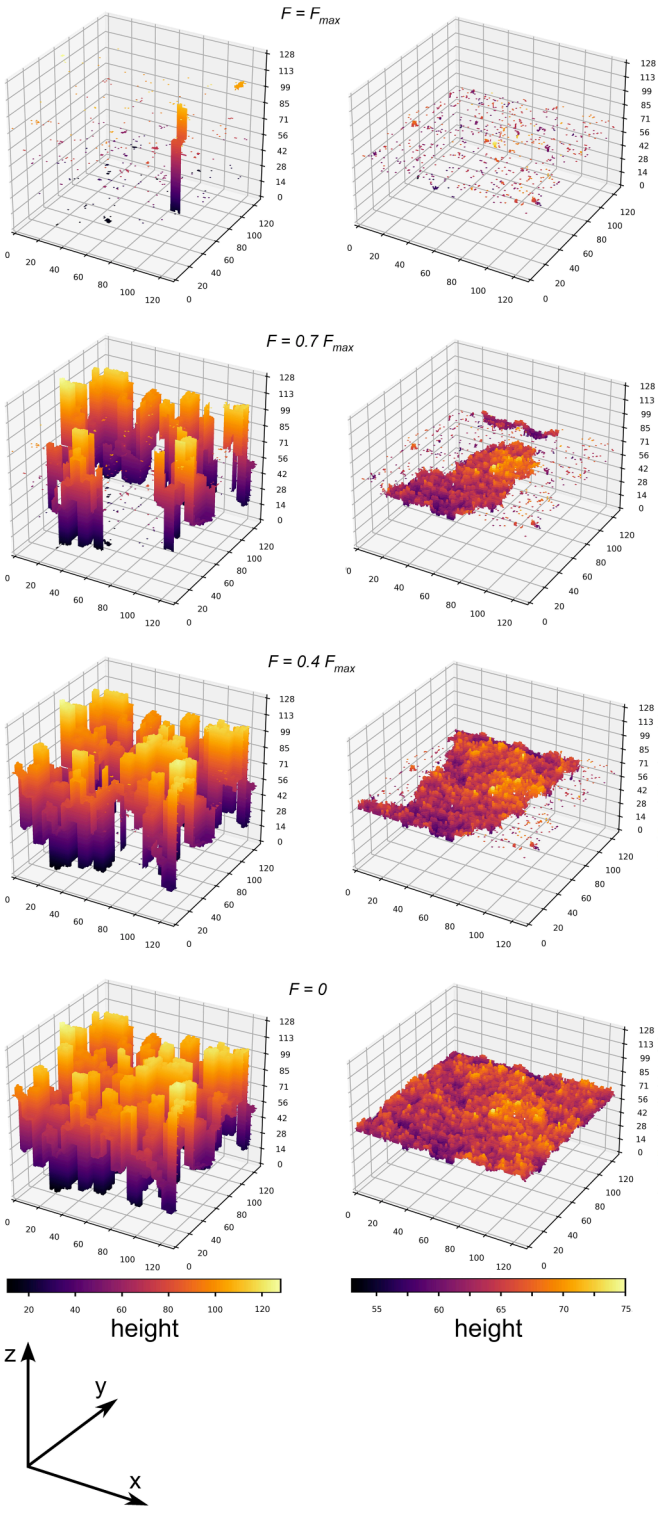

FIG. 6. Typical damage growth patterns in systems of size $L \times L \times L$ with $L = 128$, from the system's peak load (top) to global failure (bottom). The color bars indicate height (z coordinate of fracture surface). Left: DHBL. Right: RBL.

exclusively on structural considerations. The apparent exponent in our simulations is slightly lower than 1 ($H = 0.9$) due to finite-size and boundary effects, and as a consequence, the scaling behavior is limited to small r and saturates for larger

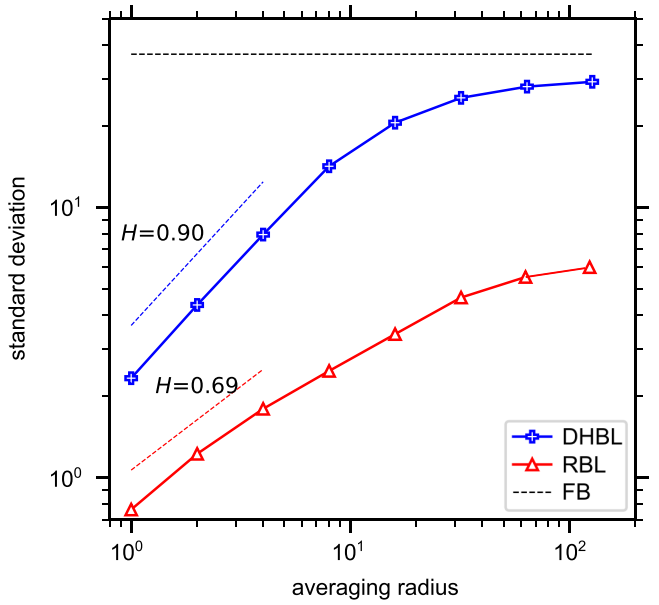

FIG. 7. Standard deviation σ_r vs averaging radius r for different 3D lattice variants.

r once the scale-dependent standard deviation reaches a value comparable to that of a completely uncorrelated, random fracture surface. To illustrate this point, Fig. 7 also shows the value $\sigma_r = L/\sqrt{12}$ for an equal load sharing fiber bundle model with fibers of length L, obtained under the assumption that $\bar{z}(\bar{x}, \bar{y})$ values are completely random variables in the interval $[0, L]$.

In order to further explore the origin of H in DHBL, we perform a multiscaling analysis. Denoting $\Delta(r)$ as the height difference between random points separated by a horizontal distance r in a random direction, the so-called structure factors of order m are then computed from

$$C^m(r) = \langle [\Delta(r)]^m \rangle_{A,N}^{1/m}. \tag{10}$$

A self-affine crack surface with Hurst exponent H would exhibit $C^m(r) \propto r^H$ for all m. Figure 8 confirms that, indeed, this condition is approximately met for crack profiles in nonhierarchical lattices (RBL) based on the results of a multiscaling analysis. In hierarchical lattices (DHBL), however, the scaling is not self-affine since the apparent Hurst exponent for different structural factors C^m is dependent on the exponent m, with $H_m = 1/m$.

We can thus rule out the self-affinity hypothesis for DHBL. At least under the current assumptions of local strength fluctuations (encoded in the choice of $\beta = 4$), we observe no explicit evidence of emergent behavior, and the remarkable superrough fracture surfaces encountered in these systems seem to be a direct consequence of the hierarchical structure and its fractal-like organization.

IV. CONCLUSIONS

In this paper, we presented the first simulations of a large-scale, three-dimensional model for a semibrittle fracture in biomimetic hierarchical materials, using full-tensorial constitutive laws and failure criteria. The degree of accuracy in our modeling approach allows us to draw conclusions about the fracture behavior of hierarchical materials, which, in the past, could be explored only under significant simplifications.

Our results confirm the long-standing view, originated in the context of bone fracture, according to which hierarchical microstructures arrest crack growth. Starting from this observation, we provide compelling numerical evidence of enhanced fault tolerance with respect to reference nonhierarchical systems. Our DHBL models outperform comparable random lattices, displaying higher peak loads and work of fracture when dealing with previously accumulated damage. A statistical analysis of the fracture surfaces allows us to conclude that, under our assumptions, this remarkable behavior shows little dependence on dynamic correlations and is, for the most part, controlled by the network structure.

The role played by the hierarchical microstructure, arresting crack growth and thus enhancing fault tolerance, represents a significant advantage in biomaterial modeling, as it paves the way to techniques of performance tuning based on microstructure design and synthesis. In a realistic scenario of this type, our DHBL model allows the parametrization of an additively manufactured hierarchical network of brittle beams or struts by acting on (i) the Weibull distribution exponents β to control the spread in local strength fluctuations and (ii)

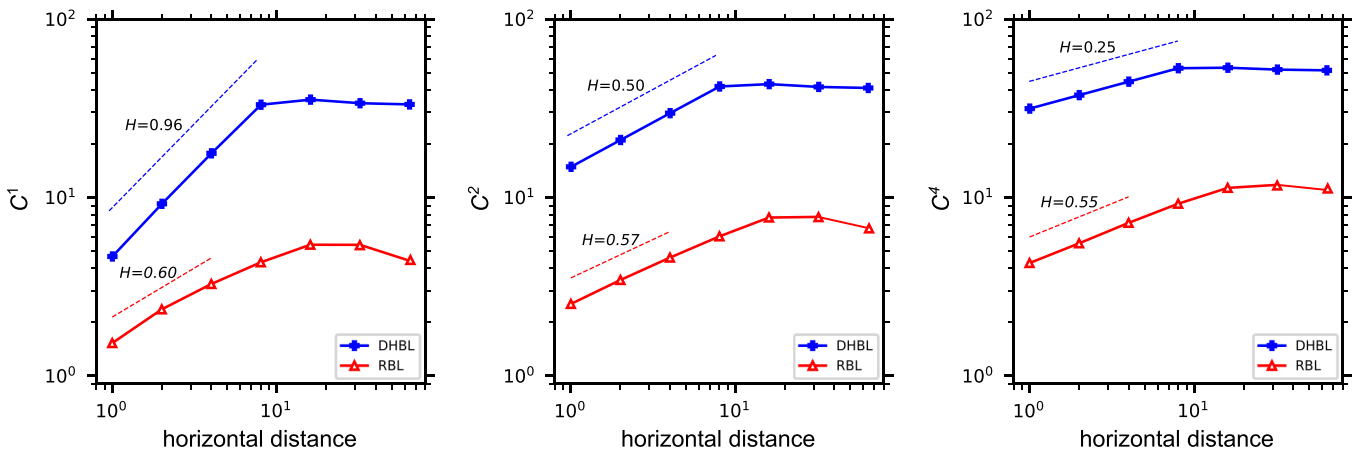

FIG. 8. Structure factors C^m for different values of m and different 3D lattice variants.

the actual constitutive laws and failure criteria. We note that in the present work we focused on the specific value of $\beta = 4$ and on a specific choice of constitutive/failure behavior. An extensive study of the role of these additional variables is left for future work. The role of fluctuations in local strength, in particular, deserves special attention. Based on results for two-dimensional systems [9], we can expect that in the case of much larger fluctuations ($\beta \approx 1$), disorder and stochastic fluctuations might become as prominent as the hierarchical structure in shaping the fracture process.

ACKNOWLEDGMENT

The authors acknowledge support from DFG under Grants No. 1Za 171/9-1 and No. 1Za 171/9-3.

[1] A. Gautieri, S. Vesentini, A. Redaelli, and M. J. Buehler, Hierarchical structure and nanomechanics of collagen microfibrils from the atomistic scale up, Nano Lett. **11**, 757 (2011).
[2] H. S. Gupta, J. Seto, W. Wagermaier, P. Zaslansky, P. Boesecke, and P. Fratzl, Cooperative deformation of mineral and collagen in bone at the nanoscale, Proc. Natl. Acad. Sci. USA **103**, 17741 (2006).
[3] M. E. Launey, M. J. Buehler, and R. O. Ritchie, On the mechanistic origins of toughness in bone, Annu. Rev. Mater. Res. **40**, 25 (2010).
[4] P. Fratzl and R. Weinkamer, Nature's hierarchical materials, Prog. Mater. Sci. **52**, 1263 (2007).
[5] D. Jiao, Z. Liu, Z. Zhang, and Z. Zhang, Intrinsic hierarchical structural imperfections in a natural ceramic of bivalve shell with distinctly graded properties, Sci. Rep. **5**, 12418 (2015).
[6] H. Gao, Application of fracture mechanics concepts to hierarchical biomechanics of bone and bone-like materials, Int. J. Fract. **138**, 101 (2006).
[7] H. Yao and H. Gao, Multi-scale cohesive laws in hierarchical materials, Int. J. Solids Struct. **44**, 8177 (2007).
[8] R. Hovden, S. E. Wolf, M. E. Holtz, F. Marin, D. A. Muller, and L. A. Estroff, Nanoscale assembly processes revealed in the nacroprismatic transition zone of *Pinna nobilis* mollusc shells, Nat. Commun. **6**, 10097 (2015).
[9] S. A. Hosseini, P. Moretti, D. Konstantinidis, and M. Zaiser, Beam network model for fracture of materials with hierarchical microstructure, Int. J. Fract. **227**, 243 (2021).
[10] M. Zaiser, S. A. Hosseini, P. Moretti, T. Mäkinen, J. Koivisto, M. Pournajar, M. Himmler, M. Redel, D. W. Schubert, and M. J. Alava, Hierarchical Slice Patterns Inhibit Crack Propagation in Brittle Sheets, Phys. Rev. Appl. **18**, 044035 (2022).
[11] P. Moretti, B. Dietemann, N. Esfandiary, and M. Zaiser, Avalanche precursors of failure in hierarchical fuse networks, Sci. Rep. **8**, 12090 (2018).
[12] N. Esfandiary, M. Zaiser, and P. Moretti, Statistical aspects of interface adhesion and detachment of hierarchically patterned structures, J. Stat. Mech. (2022) 023301.
[13] M. Pournajar, M. Zaiser, and P. Moretti, Edge betweenness centrality as a failure predictor in network models of structurally disordered materials, Sci. Rep. **12**, 11814 (2022).
[14] S. Pradhan, A. Hansen, and B. K. Chakrabarti, Failure processes in elastic fiber bundles, Rev. Mod. Phys. **82**, 499 (2010).
[15] F. Kun, S. Zapperi, and H. Herrmann, Damage in fiber bundle models, Eur. Phys. J. B **17**, 269 (2000).
[16] R. C. Hidalgo, F. Kun, and H. J. Herrmann, Creep rupture of viscoelastic fiber bundles, Phys. Rev. E **65**, 032502 (2002).
[17] F. Raischel, F. Kun, and H. J. Herrmann, Failure process of a bundle of plastic fibers, Phys. Rev. E **73**, 066101 (2006).
[18] N. M. Pugno, F. Bosia, and T. Abdalrahman, Hierarchical fiber bundle model to investigate the complex architectures of biological materials, Phys. Rev. E **85**, 011903 (2012).
[19] S. Biswas and M. Zaiser, Avalanche dynamics in hierarchical fiber bundles, Phys. Rev. E **100**, 022133 (2019).
[20] A. Nova, S. Keten, N. M. Pugno, A. Redaelli, and M. J. Buehler, Molecular and nanostructural mechanisms of deformation, strength and toughness of spider silk fibrils, Nano Lett. **10**, 2626 (2010).
[21] M. J. Alava, P. K. V. V. Nukala, and S. Zapperi, Statistical models of fracture, Adv. Phys. **55**, 349 (2006).
[22] C. Manzato, A. Shekhawat, P. K. V. V. Nukala, M. J. Alava, J. P. Sethna, and S. Zapperi, Fracture Strength of Disordered Media: Universality, Interactions, and Tail Asymptotics, Phys. Rev. Lett. **108**, 065504 (2012).
[23] P. K. V. V. Nukala and S. Simunovic, A continuous damage random thresholds model for simulating the fracture behavior of nacre, Biomaterials **26**, 6087 (2005).
[24] J. Sun and B. Bhushan, Hierarchical structure and mechanical properties of nacre: A review, RSC Adv. **2**, 7617 (2012).
[25] P. K. V. V. Nukala, S. Zapperi, M. J. Alava, and S. Šimunović, Crack roughness in the two-dimensional random threshold beam model, Phys. Rev. E **78**, 046105 (2008).
[26] S. A. Hosseini, P. Moretti, and M. Zaiser, A beam network model approach to strength optimization of disordered fibrous materials, Adv. Eng. Mater. **22**, 1901013 (2020).
[27] See Supplemental Material at http://link.aps.org/supplemental/10.1103/PhysRevMaterials.7.053612 for typical damage growth patterns for different lattice variants.
[28] S. A. Hosseini, Fracture and failure properties of hierarchical materials, Ph.D. thesis, Friedrich-Alexander-Universität Erlangen-Nürnberg, 2022.
[29] J. Przemieniecki, *Theory of Matrix Structural Analysis* (Dover, New York, 1985).
[30] A. C. Ugural, *Advanced Mechanics of Materials and Applied Elasticity* (Prentice Hall, Upper Saddle River, NJ, 2012).
[31] J. DeWolf, D. Mazurek, F. Beer, and E. Johnston, *Mechanics of Materials* (McGraw-Hill Education, New York, 2014).
[32] P. K. V. V. Nukala, P. Barai, S. Zapperi, M. J. Alava, and S. Šimunović, Fracture roughness in three-dimensional beam lattice systems, Phys. Rev. E **82**, 026103 (2010).
[33] M. J. Alava, P. K. V. V. Nukala, and S. Zapperi, Role of Disorder in the Size Scaling of Material Strength, Phys. Rev. Lett. **100**, 055502 (2008).
[34] H. Tada, P. C. Paris, and G. R. Irwin, *The Stress Analysis of Cracks Handbook*, 3rd ed. (ASME Press, New York, 2000).
[35] A. Hansen, E. L. Hinrichsen, and S. Roux, Roughness of Crack Interfaces, Phys. Rev. Lett. **66**, 2476 (1991).